ACS NANO
Cite This: ACS Nano XXXX, XXX, XXX−XXX
www.acsnano.org

ARTICLE

Nickel Adatoms Induced Tautomeric Dehydrogenation of Thymine Molecules on Au(111)

Huihui Kong,[†,‡] Chi Zhang,[†] Qiang Sun,[†] Xin Yu,[†] Lei Xie,[†] Likun Wang,[†] Lei Li,[§] Shanwei Hu,[∥] Huanxin Ju,[∥] Yunbin He,[§] Junfa Zhu,[∥] and Wei Xu*[,†]

[†]Interdisciplinary Materials Research Center, Tongji-Aarhus Joint Research Center for Nanostructures and Functional Nanomaterials, College of Materials Science and Engineering, Tongji University, Shanghai 201804, P. R. China

[‡]Herbert Gleiter Institute of Nanoscience, School of Materials Science and Engineering, Nanjing University of Science and Technology, Xiaolingwei 200, Nanjing 210094, Jiangsu, P. R. China

[§]Ministry of Education Key Laboratory of Green Preparation and Application for Functional Materials, School of Materials Science and Engineering, Hubei University, Wuhan 430062, P. R. China

[∥]National Synchrotron Radiation Laboratory, University of Science and Technology of China, Hefei 230029, P. R. China

S *Supporting Information*

ABSTRACT: **Tautomerization of nucleobases may induce base mismatches resulting in the abnormal disturbance of gene replication and expression, which has therefore attracted widespread interests in many disciplines. Metal atoms participating in a variety of important biological processes are found to be able to affect the nucleobase tautomerization as evidenced by many theoretical and spectroscopic studies. To get the real-space evidence and to unravel the underlying mechanism for the metal-induced tautomerization, especially from the keto form to the enol one, the interplay of high-resolution scanning tunneling microscopy imaging/manipulation and density functional theory (DFT) calculations has been employed. We present a process showing the Ni adatom-induced keto−enol tautomeric dehydrogenation of thymine molecules on Au(111). The key to making such a process feasible is the Ni atoms which greatly lower the energy barrier for the tautomerization from keto to enol form, which is rationalized by extensive DFT-based transition-state search calculations.**

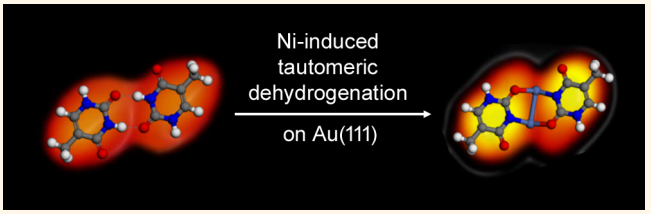

KEYWORDS: *scanning tunneling microscopy, density functional theory, tautomeric dehydrogenation, thymine, nickel adatom*

Tautomerization, involving the transfer of a proton or hydrogen atom of organic compounds, is a pervasive phenomenon in biomolecules (*e.g.*, amino acids and nucleobases)[1,2] and has significant impacts on various functions of biomolecules in working biosystems. Generally, nucleobases exist in their canonical forms *in vivo* which give rise to the so-called Watson−Crick base pairing and further govern high-fidelity replications of DNA molecules.[3] Nevertheless, tautomerization of nucleobases may induce base mismatches resulting in the abnormal disturbance of gene replication and expression.[4] In view of the potential biological significance of nucleobase tautomerizations, a number of studies have been performed to investigate the possible tautomeric species and their relative stabilities under various external stimuli. Among others, water[5−8] has been proven to play an important role in affecting the tautomeric stabilities of nucleobases and further influencing the existence of non-canonical tautomeric forms. Besides, metal atoms participating in a variety of important biological processes are also found to be able to affect the nucleobases tautomerization as reported by many theoretical and spectroscopic studies.[9−12] Moreover, it has been theoretically proposed that the stability orders of nucleobase tautomers could be greatly altered by the delicate selection of different metal species.[13,14] Recently, scanning tunneling microscopy (STM) has been employed to study the roles of metals on the nucleobase tautomerization and revealed that (i) Ni atoms are able to inhibit the formation of the noncanonical G/7H form of guanine (G) molecules[15] and (ii) Na atoms could promote the conversion from the non-canonical G/7H form of G molecules to the canonical G/9H one.[16] Most of the real-space studies are focused on the formation of canonical forms of nucleobases, metal-induced tautomerization from canonical forms to noncanonical ones,

Received: April 16, 2018
Accepted: August 21, 2018
Published: August 21, 2018

DOI: 10.1021/acsnano.8b02821
ACS Nano XXXX, XXX, XXX−XXX

especially the well-known keto−enol tautomerization of nucleobases has been less addressed.[17−21] It is therefore of general interest to explore the metal-induced keto−enol tautomerization of nucleobases and, more importantly, to unravel the underlying reaction mechanism.

In this study, we choose a thymine (T) molecule as a potential candidate to interact with metal atoms. As T molecules contain diketo groups (O2, O4) locating close to two imino groups (N1, N3) (as illustrated in Figure 1), it thus provides us a model system to explore the keto−enol tautomerization. Subsequently, Ni atoms are selected to induce the potential keto−enol tautomerization of the T molecule on the basis of the following considerations: Ni atoms preferentially coordinate to nitrogen atoms in comparison with oxygen atoms,[15,18] which may catalyze the proton transfer from the imino to the keto group thus inducing the keto−enol tautomerization. The Au(111) surface is chosen as the template for the following reasons: In comparison with copper surfaces, the Au(111) surface is relatively inert and normally does not provide a lot of adatoms which may directly coordinate with organic molecules. Besides, the corrugation of the potential energy surface of Au(111) is sufficiently small, allowing the molecules to easily diffuse on the surface and form the self-assembled structures. On the other hand, the surface itself can also be treated as a catalyst due to the 2D confinement effect when molecules adsorbed on that, which has shown to be able to lower the activation energy barriers of *in situ* chemical reactions. From the interplay of high-resolution STM imaging/manipulation and density functional theory (DFT) calculations, we have explored a process showing Ni adatoms induced tautomerization (*i.e.*, from keto (T/3 NH) form to enol (T/4 OH) one) and subsequent dehydrogenation (enol T/4 O) of thymine molecules on Au(111) (*cf.* Figure 1). The possible reaction pathways have also been rationalized by DFT calculations, and the key to making such a tautomeric dehydrogenation process feasible is the Ni atoms which greatly lower the energy barrier for the tautomerization from keto (T/3 NH) to enol (T/4 OH) and subsequently slightly facilitate the dehydrogenation of enol (T/4 OH).

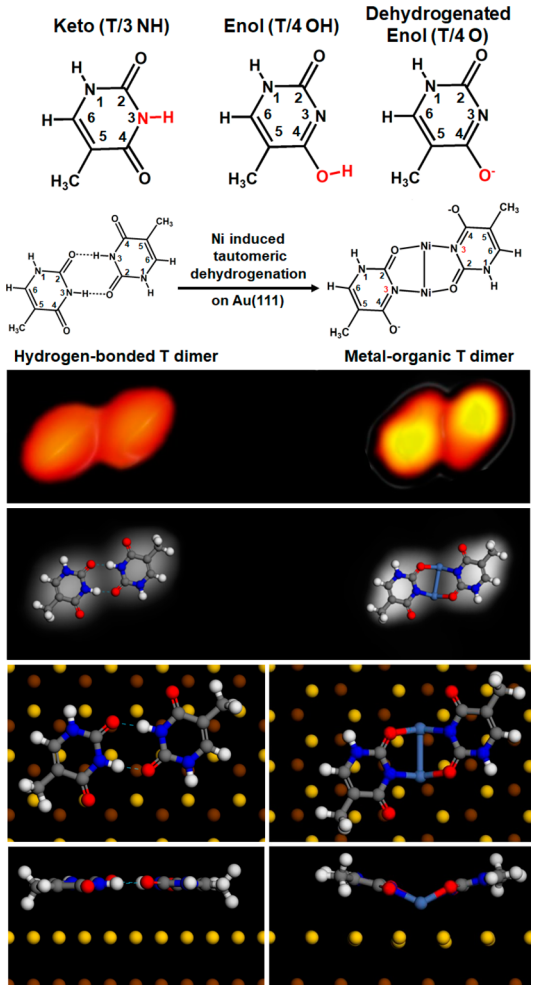

Figure 1. Upper panel: Schematic illustration on the chemical structure of the canonical keto form T/3 NH, the most stable noncanonical enol form T/4 OH, and dehydrogenated enol form T/4 O, and schematic illustration on the hydrogen-bonded T dimer and the metal−organic T dimer. Middle panel: Close-up STM images and the corresponding STM simulations superimposed with optimized models of hydrogen-bonded and metal−organic T dimers. Lower panel: The corresponding top and side views of the optimized models on Au(111). C, gray; N, blue; O, red; H, white; Ni, indigo blue; Au, yellow (first layer) or brown (second layer). Tunneling parameters for the left and right STM image in the middle panel are V_t = 1.25 V, I_t = 0.47 nA and V_t = 1.23 V, I_t = 0.79 nA. The bias for STM simulation is 1.2 V.

RESULTS AND DISCUSSION

Deposition of T molecules on Au(111) held at room temperature (RT) leads to the formation of previously reported hydrogen-bonded T chains (Figure 2a).[22] From the high-resolution STM image (Figure 2b) together with the overlaid DFT optimized model (Figure 2c), we identify that the chains are composed of hydrogen-bonded T dimers (as indicated by the blue contour in Figure 2b), where the T molecules are in the canonical form. The canonical form of T molecules is further verified by synchrotron radiation photoemission spectroscopy (SRPES) experiment, as shown in Figure S1a,b in Supporting Information, which show single peak for N 1s (B.E. = 399.8 eV) and O 1s (B.E. = 531.0 eV) that should be attributed to N−H and C═O species, respectively.[23] The SRPES data unambiguously reveals that there are only N−H and C═O groups in the hydrogen-bonded T chains, and no peaks related to pyridine N or −OH groups are observed, which indicates that no keto−enol tautomerization is involved within the hydrogen-bonded T chains. Such self-assembled T chains stay unchanged after annealing until the T molecules desorb from the Au(111) surface.

Interestingly, if we introduce Ni atoms into the hydrogen-bonded T chains with post-annealing at 390 K, another kind of chain structure is formed as shown in Figure 2d. From the close-up STM image (Figure 2e), we identify that such a hybrid chain is composed of two kinds of alternating T dimers, that is, the dim one (indicated by the blue contour) and the bright one (indicated by the green contour). Closer inspection allows us to identify that the dim ones resemble the hydrogen-bonded T dimers both in the apparent height and the morphology (*cf.* Figure S3), which should therefore be assigned to hydrogen-bonded T dimers. The bright ones are speculated to be related to metal−organic structures since they never appeared before introducing Ni atoms. Based on the above analysis, detailed DFT calculations including the Au(111) substrate were carried out to unravel the atomic-scale structures of the bright dimer and the hybrid chain. After

DOI: 10.1021/acsnano.8b02821
ACS Nano XXXX, XXX, XXX−XXX

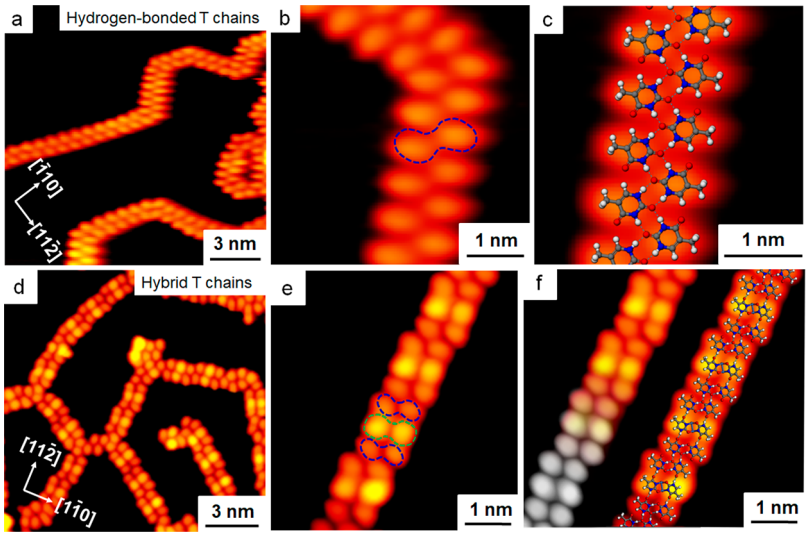

Figure 2. (a–c) STM images showing the formation of hydrogen-bonded T chains at RT on Au(111). (a) Large-scale and (b) high-resolution STM images showing that the chains are formed by the T dimer as indicated by the blue contour in (b). (c) The close-up STM image overlaid with the DFT optimized model showing the chain is composed of hydrogen-bonded T dimers that are in the canonical form. (d–f) STM images showing the formation of hybrid T chains after introducing Ni atoms and post-annealing at 390 K. (d) Large-scale and (e) high-resolution STM images showing that the hybrid chains are formed by two kinds of alternating dimers as indicated by blue and green contours, respectively. (f) The STM image overlaid with the DFT optimized model and the simulated STM image showing the chain is composed of hydrogen-bonded T dimers in the canonical forms and the metal–organic T dimers in the tautomerically dehydrogenated form. Tunneling parameters: (a–c) V_t = 1.25 V, I_t = 0.47 nA; (d–f): V_t = 1.25 V, I_t = 0.67 nA. The bias for STM simulation is 1.2 V.

an extensive structural search and comparison with high-resolution STM images, we finally get an energetically favorable model for the bright dimer as shown in Figure 1. From this DFT relaxed model, we distinguish that the chemical structure of T molecules has transformed from the canonical keto (T/3 NH) form to the dehydrogenated enol (T/4 O) one. After coordinating with Ni atoms, the molecules adopt a slightly tilt adsorption configuration (*cf.* Figure 1), which rationally accounts for the bright appearance of metal–organic T dimers. These metal–organic T dimers and hydrogen-bonded T dimers are further connected by two N–H···O hydrogen bonds forming the observed hybrid chains, which is also rationalized by the DFT optimized model and the STM simulation (Figure 2f).

From the model of hybrid chains, we speculate that the formation of metal–organic T chains would be possible if we remove the hydrogen-bonded T dimers without perturbing the metal–organic T dimers. Expectedly, annealing the hybrid chain structures at 410 K for 15 min indeed results in the formation of pure metal–organic T chains as shown in Figure 3a, which is also rationalized by the DFT optimized model and the STM simulation as shown in Figure 3b. STM manipulations allow us to controllably remove a metal–organic T dimer from the chain (Figure 3c) or induce a dislocation of the T dimer as a whole (Figure 3d). These processes also indicate that the metal–organic interaction within the T dimer is stronger than the hydrogen bonds in between the T dimers. It should be mentioned that the dislocation of metal–organic T dimers with respect to the straight chain also exists in the original metal–organic chains, as shown in Figure S4, and such a configuration is also stabilized by the double N–H···O^- hydrogen bonds between the T dimers. From the model in Figure 3b, the metal–organic dimers are formed by two dehydrogenated T/4 O molecules coordinating with two Ni atoms at N3 and O2 site, and then the metal–organic T dimers bind together by the N(1)–H···

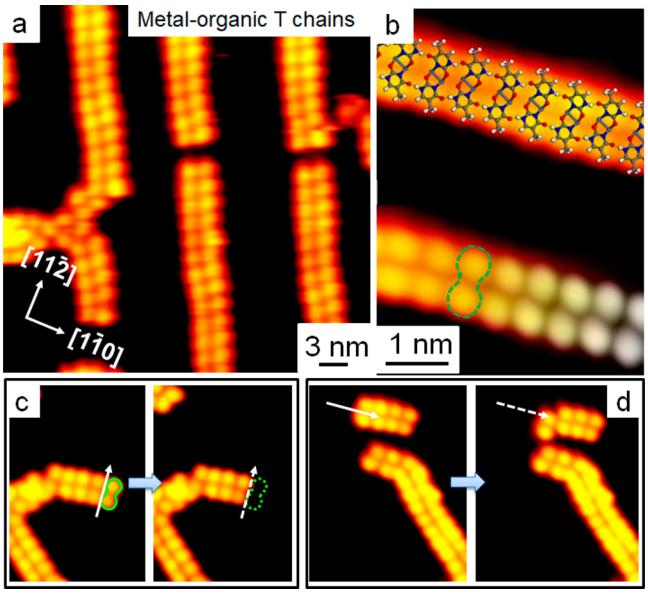

Figure 3. STM images showing the formation of metal–organic T chains after annealing the hybrid chain-covered surface at 410 K. (a) Large-scale and (b) high-resolution STM images overlaid with the DFT optimized model and the simulated STM image showing that the chains are formed by the metal–organic T dimer as indicated by the green contour in (b). (c, d) Lateral STM manipulations showing the metal–organic T dimer moving as a whole. Tunneling parameters: (a–d) V_t = 1.23 V, I_t = 0.79 nA. The bias for STM simulation is 1.2 V.

$O(4)^-$ hydrogen bonds to form the observed metal–organic T chains. To further verify such a model, we performed SRPES analysis on the metal–organic T chains, as shown in Figure S1. Compared with one single peak of N 1s within hydrogen-bonded T chains, the N 1s core level spectrum of the metal–organic T chains was fitted with two peaks (B.E. = 400.5 and

DOI: 10.1021/acsnano.8b02821
ACS Nano XXXX, XXX, XXX–XXX

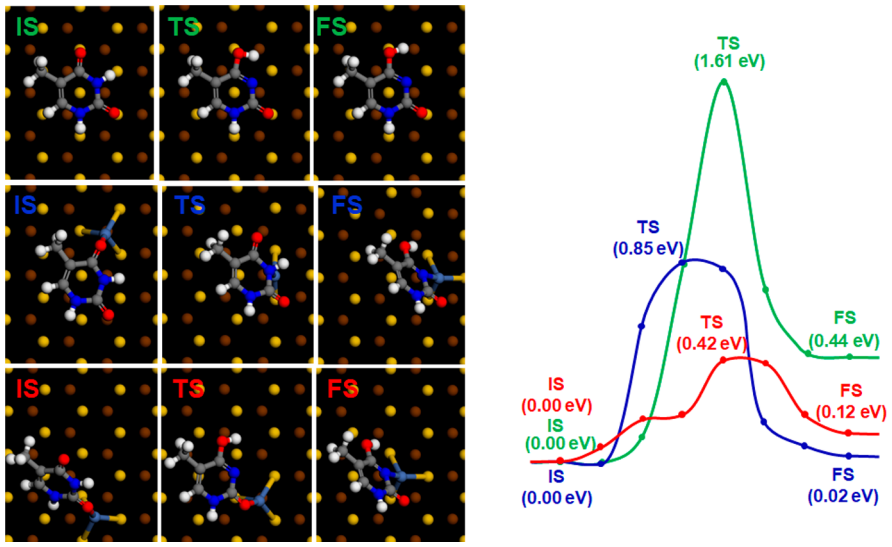

Figure 4. DFT calculated reaction pathways for the tautomerization process from keto T/3 NH to enol T/4 OH without and with the Ni atom on Au(111). DFT calculated pathways without Ni, with Ni coordinating with O4 as the initial state, and with Ni coordinating with O2 as the initial state are indicated by green, blue, and red lines in the right panel, respectively, and the corresponding models are shown in the left panel. Relative energies of the local minima (initial state (IS), final state (FS)) and the transition states (TS) along the reaction path are given with respect to the IS.

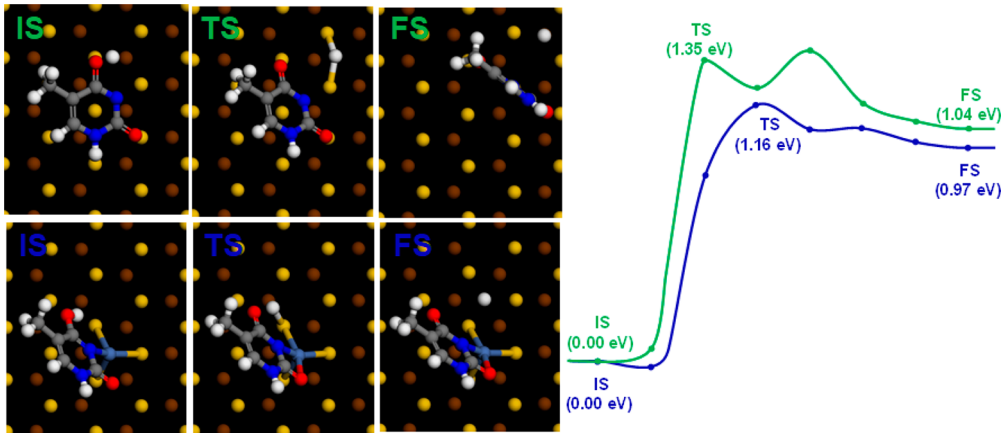

Figure 5. DFT calculated reaction pathways for the dehydrogenation process from enol T/4 OH to T/4 O without (see the green line) and with (see the blue line) the Ni atom on Au(111). Relative energies of the local minima (IS, FS) and the transition states (TS) along the reaction path are given with respect to the initial state IS. The corresponding models are shown in the upper and lower panels in the left panel, respectively.

398.9 eV with equal intensity). The contributions for the binding energy of 400.5 eV/398.9 eV should be assigned to the pyridine N coordinating with Ni atoms[24] and N−H group forming strong N−H···O$^-$ hydrogen bonds.[25] The appearance of the pyridine N-related peak indicates that keto−enol tautomerization occurs.

Similarly, we also observed two predominant peaks of O 1s core level spectrum (B.E. = 531.4 eV/530.5 eV), which should be attributed to C═O group coordinating with Ni atoms[25] and C−O$^-$ group forming N−H···O$^-$ hydrogen bonds.[26] Again, no apparent peak related to −OH groups is observed indicating dehydrogenation of T molecules from T/4 OH to T/4 O. The combination of N 1s and O 1s SRPES data reveals that the introduction of Ni atoms should have induced the tautomeric dehydrogenation of T molecules from T/3 NH to T/4 O.

To unravel the underlying mechanism for such a nickel-induced tautomeric dehydrogenation process, extensive DFT-based transition-state searches are carried out to discover possible reaction pathways. First, we calculate the possible reaction pathways for direct dehydrogenation from the canonical T/3 NH form to T/3 N on Au(111) without and with Ni atoms as shown in Figure S5. The calculated reaction energy barriers for these two processes are determined to be 2.07 and 1.88 eV, respectively, which is obviously too high in comparison with the experimental conditions (annealing the sample at 390 K). According to the previous study by Furukawa *et al.*,[20] tautomeric dehydrogenation reaction is proposed to occur on guanine (G) molecules due to the existence of the neighboring keto group (C═O) and imino group (N−H). Inspired from that, we speculate that the tautomeric dehydrogenation of T molecules might also undergo similar processes due to the similar peripheral functional groups.

On the basis of the above speculation, DFT-based transition-state searches are further performed to figure out a rational

DOI: 10.1021/acsnano.8b02821
ACS Nano XXXX, XXX, XXX−XXX

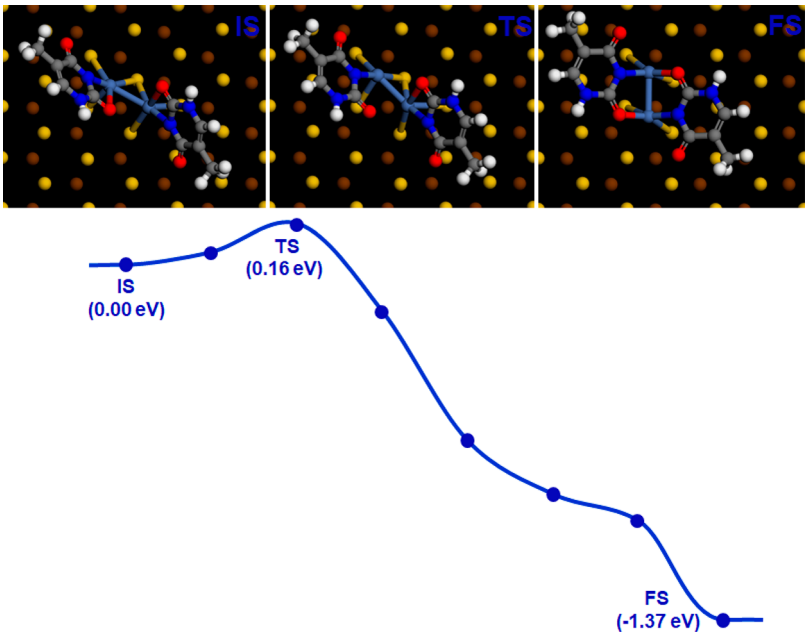

Figure 6. DFT calculated reaction pathway for the formation of a metal−organic T dimer on Au(111). Relative energies of the local minima (IS, FS) and the transition state (TS) along the reaction path are given with respect to the initial state IS.

tautomeric dehydrogenation process. First, we calculated the possible reaction pathways for the tautomerization from keto T/3 NH to enol T/4 OH without and with Ni atoms on Au(111) as shown in Figure 4. It is seen that the calculated energy barrier for this tautomerization process is determined to be 1.61 eV without the Ni atom (*cf.* the green line). While, interestingly, by introduction of a Ni atom into this process, the energy barriers dramatically decrease to 0.85 eV (*cf.* the blue line) or 0.42 eV (*cf.* the red line), respectively, depending on the initial coordination site between the T molecule and the Ni atom. Second, we calculate the energy barrier for the dehydrogenation process from enol T/4 OH to T/4 O without and with the Ni atom on Au(111) as shown in Figure 5. It is found that the energy barrier is also reduced from 1.35 eV (*cf.* the green line) to 1.16 eV (*cf.* the blue line) with the assistance of the Ni atom. Finally, we calculate the energy barrier for the formation of a metal−organic T dimer on Au(111) as shown in Figure 6. The energy barrier is determined to be only 0.16 eV, and this process is exothermic by 1.37 eV, which indicates the formation of experimentally observed metal−organic T dimers experiencing from a Ni-induced tautomeric dehydrogenation process is thermodynamically favorable on the Au(111) surface.

The presented data are performed under well controlled UHV conditions on a single crystal surface, which is a rather simplified model system in comparison with the real biological system. From the literature,[27] it was shown that the Ni often exists in the form of Ni^{2+} in cells. From our XPS experiments and Bader charge analysis (*cf.* Figure S1 and S2), it is shown that Ni is positively charged by +0.67 e within the metal−organic T chains on Au(111). To further mimic the biologically relevant system, we need to consider the influence of other factors, like water. Along this direction, we have previously studied the role of water in other nucleobase-related systems and identified the rare guanine tautomer induced by water.[8] Also, from the literature,[28] it was shown that water-soluble Ni salts penetrated cells poorly and therefore were not carcinogenic in many living bodies, which indicated that water may play positive roles in inhibiting the water-soluble Ni salts to attack cells and further induce DNA damage. The Ni^{2+} existed in the form of hydrated ions in cells. The hydrated Ni^{2+} has been proven to have no effect on DNA damage,[29] but the introduction of H_2O_2 may induce DNA damage. So, it would be very interesting to further introduce H_2O or H_2O_2 into the system investigated here to study the role of Ni together with water in the nucleobases tautomerization.

CONCLUSION

In conclusion, from the interplay of high-resolution STM imaging/manipulation and systematic DFT calculations together with SRPES/XPS experiments, we have provided real-space experimental evidence on the metal-induced tautomeric dehydrogenation process. These findings provide fundamental hints into the role of metals in affecting the nucleobase tautomerization, which may also help to gain deeper understandings of more biologically relevant processes from a single-molecule level.

METHODS AND MATERIALS

All STM experiments were performed in a UHV chamber (base pressure 1×10^{-10} mbar) equipped with the variable-temperature, fast-scanning "Aarhus-type" STM,[30,31] a molecular evaporator and an e-beam evaporator, and other standard facilities for sample preparation. The Au(111) substrate was prepared by several cycles of 1.5 keV Ar^+ sputtering, followed by annealing to 830 K for 15 min resulting in clean and flat terraces separated by monatomic steps. The thymine molecules (purchased from Sigma-Aldrich with purity >98%) were loaded into a quartz crucible in the molecular evaporator. After a thorough degassing, thymine molecules were solely deposited or thymine molecules and Ni atoms were co-deposited onto the clean Au(111) surface held at RT. During deposition of thymine molecules, the molecular evaporator was held at 350 K. There is no thermocouple connected with e-beam evaporator, and we deposit Ni atoms by keeping the emission current at about 8 mA and the high voltage at 1.0 kV for 1 min. The sample was thereafter transferred within the UHV chamber to the STM, where measurements were carried out over a temperature range of 120−150 K to stabilize the

DOI: 10.1021/acsnano.8b02821
ACS Nano XXXX, XXX, XXX−XXX

formed nanostructures. The electrochemically etched, polycrystalline W STM-tip was used for collection of data in this manuscript. The lateral manipulations were carried out in a controllable line-scan mode under specific scanning conditions (by increasing the tunnel current up to approximately 2.0 nA while reducing the tunnel voltage down to approximately 10 mV). During annealing of the sample, the temperature is detected by a thermocouple connecting on the heating stage.

The calculations were performed in the framework of DFT by using the Vienna ab initio simulation package (VASP).[32,33] The projector augmented wave method was used to describe the interaction between ions and electrons,[34,35] and the Perdew–Burke–Ernzerhof generalized gradient approximation exchange–correlation functional was employed,[36] and van der Waals (vdW) interactions were included using the dispersion-corrected DFT-D3 method of Grimme.[37] The atomic structures were relaxed using the conjugate gradient algorithm scheme as implemented in the VASP code until the forces on all unconstrained atoms were ≤0.03 eV/Å. The simulated STM images were obtained by the Hive program based on the Tersoff–Hamann method. The climbing image nudged elastic band was applied to locate the transition state, and the transition path was optimized until the forces acting on the path were typically ≤0.03 eV/Å. The unit cells of DFT calculations for hydrogen-bonded T dimer and metal–organic one in Figure 1 are a = 1.32 nm, b = 1.52 nm, α = 90° and a = 2.02 nm, b = 2.02 nm, α = 90°, respectively. The unit cells of DFT calculations in Figure 2c,d are a = 1.32 nm, b = 1.52 nm, α = 90° and a = 2.08 nm, b = 2.08 nm, α = 92.2°, respectively. The unit cell of DFT calculations in Figure 3 is a = 1.26 nm, b = 1.89 nm, α = 104.18°. The unit cells in Figures 4 and 5 are a = 1.44 nm, b = 1.44 nm, α = 120°; a = 1.32 nm, b = 1.52 nm, α = 90°, respectively. The unit cell in Figure 6 is a = 2.02 nm, b = 144 nm, α = 120°.

The SRPES experiments were performed at the Catalysis and Surface Science Endstation at the BL11U beamline in the National Synchrotron Radiation Laboratory (NSRL) in Hefei, China.[38] The sample was transferred from the STM chamber to the endstation by a transport suitcase with a getter pump to keep the pressure under 5×10^{-9} mbar. The core level spectra of N 1s, O 1s were recorded with a VG Scienta R4000 analyzer using synchrotron radiation light. N 1s, O 1s core level spectra were taken with photon energies of 500 and 590 eV, respectively. The photon energies were calibrated and referenced to the Au binding energy of a sputter-cleaned Au substrate. Before every scan of the N 1s and O 1s spectra, we also measured the Au binding energy of the Au substrate for calibration. The Ni $2p_{3/2}$ spectra were recorded with the same VG Scienta R4000 analyzer by using a monochromatic Al Kα X-ray source with the photon energy of 1486.6 eV.

ASSOCIATED CONTENT

Supporting Information

The Supporting Information is available free of charge on the ACS Publications website at DOI: 10.1021/acsnano.8b02821.

Additional STM images (PDF)

AUTHOR INFORMATION

Corresponding Author

*E-mail: xuwei@tongji.edu.cn.

ORCID

Huihui Kong: 0000-0001-5652-5269
Qiang Sun: 0000-0003-4903-4570
Yunbin He: 0000-0002-7179-4392
Junfa Zhu: 0000-0003-0888-4261
Wei Xu: 0000-0003-0216-794X

Notes

The authors declare no competing financial interest.

ACKNOWLEDGMENTS

The authors acknowledge financial supports from the National Natural Science Foundation of China (21473123, 51572073, 21622307, 21790351, 21802072), the Research Fund for Science and Technology Program of Jiangsu Province (BK20170827), and the Fundamental Research Funds for the Central Universities (no. 3091701134).

REFERENCES

(1) Topal, M. D.; Fresco, J. R. Complementary Base-Pairing and the Origin of Substitution Mutations. *Nature* **1976**, *263*, 285–289.

(2) Choi, M. Y.; Miller, R. E. Four Tautomers of Isolated Guanine from Infrared Laser Spectroscopy in Helium Nanodroplets. *J. Am. Chem. Soc.* **2006**, *128*, 7320–7328.

(3) Watson, J. D.; Crick, F. H. C. Molecular Structure of Nucleic Acids. *Nature* **1953**, *171*, 737–738.

(4) Lowdin, P. O. Proton Tunneling in DNA and Its Biological Implications. *Rev. Mod. Phys.* **1963**, *35*, 724–732.

(5) Gu, J.; Leszczynski, J. A DFT Study of the Water-Assisted Intramolecular Proton Transfer in the Tautomers of Adenine. *J. Phys. Chem. A* **1999**, *103*, 2744–2750.

(6) Hanus, M.; Ryjacek, F.; Kabelac, M.; Kubar, T.; Bogdan, T. V.; Trygubenko, S. A.; Hobza, P. Correlated *Ab Initio* Study of Nucleic Acid Bases and Their Tautomers in the Gas Phase, in a Microhydrated Environment and in Aqueous Solution. Guanine: Surprising Stabilization of Rare Tautomers in Aqueous Solution. *J. Am. Chem. Soc.* **2003**, *125*, 7678–7688.

(7) Gorb, L.; Leszczynski, J. Intramolecular Proton Transfer in Mono- and Dihydrated Tautomers of Guanine: an *Ab Initio* Post Hartree-Fock Study. *J. Am. Chem. Soc.* **1998**, *120*, 5024–5032.

(8) Zhang, C.; Xie, L.; Ding, Y.; Sun, Q.; Xu, W. Real-Space Evidence of Guanine Tautomer Induced by Water. *ACS Nano* **2016**, *10*, 3776–3782.

(9) Bagchi, S.; Mandal, D.; Ghosh, D.; Das, K. D. Density Functional Theory Study of Interaction, Bonding and Affinity of Group IIb Transition Metal Cations with Nucleic Acid Bases. *Chem. Phys.* **2012**, *400*, 108–117.

(10) Russo, N.; Toscano, M.; Grand, A. Lithium Affinity for DNA and RNA Nucleobases. The Role of Theoretical Information in the Elucidation of the Mass Spectrometry Data. *J. Phys. Chem. B* **2001**, *105*, 4735–4741.

(11) van der Wijst, T.; Guerra, C. F.; Swart, M.; Bickelhaupt, F. M.; Lippert, B. Rare Tautomers of 1-Methyluracil and 1-Methylthymine: Tuning Relative Stabilities through Coordination to Pt^{II} Complexes. *Chem. - Eur. J.* **2009**, *15*, 209–218.

(12) Rincon, E.; Yanez, M.; Toro-Labbe, A.; Mo, O. Effect of Ni(II), Cu(II) and Zn(II) Association on the Keto-Enol Tautomerism of Thymine in the Gas Phase. *Phys. Chem. Chem. Phys.* **2007**, *9*, 2531–2537.

(13) Martinez, A. Theoretical Study of Guanine-Cu and Uracil-Cu (Neutral, Anionic, and Cationic). Is It Possible to Carry Out a Photoelectron Spectroscopy Experiment? *J. Chem. Phys.* **2005**, *123*, 024311.

(14) Burda, J. V.; Sponer, J.; Hobza, P. *Ab Initio* Study of the Interaction of Guanine and Adenine with Various Mono- and Bivalent Metal Cations (Li^+, Na^+, K^+, Rb^+, Cs^+; Cu^+, Ag^+, Au^+; Mg^{2+}, Ca^{2+}, Sr^{2+}, Ba^{2+}; Zn^{2+}, Cd^{2+}, and Hg^{2+}). *J. Phys. Chem.* **1996**, *100*, 7250–7255.

(15) Kong, H.; Sun, Q.; Wang, L.; Tan, Q.; Zhang, C.; Sheng, K.; Xu, W. Atomic-Scale Investigation on the Facilitation and Inhibition of Guanine Tautomerization at Au(111) Surface. *ACS Nano* **2014**, *8*, 1804–1808.

(16) Zhang, C.; Xie, L.; Wang, L.; Kong, H.; Tan, Q.; Xu, W. Atomic-Scale Insight into Tautomeric Recognition, Separation and Interconversion of Guanine Molecular Networks on Au(111). *J. Am. Chem. Soc.* **2015**, *137*, 11795–11800.

(17) Papageorgiou, A. C.; Fischer, S.; Reichert, J.; Diller, K.; Blobner, F.; Klappenberger, F.; Allegretti, F.; Seitsonen, A. P.; Barth, J.

DOI: 10.1021/acsnano.8b02821
ACS Nano XXXX, XXX, XXX–XXX

V. Chemical Transformations Drive Complex Self-Assembly of Uracil on Close-Packed Coinage Metal Surfaces. *ACS Nano* **2012**, *6*, 2477−2486.
(18) Kong, H.; Wang, L.; Sun, Q.; Zhang, C.; Tan, Q.; Xu, W. Controllable Scission and Seamless Stitching of Metal-Organic Clusters by STM Manipulation. *Angew. Chem., Int. Ed.* **2015**, *54*, 6526−6530.
(19) McNutt, A.; Haq, S.; Raval, R. High Temperature Phase of the DNA Base Thymine on Cu(110): A Resonance Delocalised Bonding System. *Surf. Sci.* **2002**, *502*, 185−192.
(20) Furukawa, M.; Yamada, T.; Katano, S.; Kawai, M.; Ogasawara, H.; Nilsson, A. Geometrical Characterization of Adenine and Guanine on Cu(110) by NEXAFS, XPS, and DFT Calculation. *Surf. Sci.* **2007**, *601*, 5433−5440.
(21) Lopez, A.; Chen, Q.; Richardson, N. V. Combined STM, HREELS and *Ab Initio* Study of the Adsorption of Uracil on Si(100)-2 × 1. *Surf. Interface Anal.* **2002**, *33*, 441−446.
(22) Xu, W.; Kelly, R. E. A.; Otero, R.; Schock, M.; Lægsgaard, E.; Stensgaard, I.; Kantorovich, L. N.; Besenbacher, F. Probing the Hierarchy of Thymine-Thymine Interactions in Self-Assembled Structures by Manipulation with Scanning Tunneling Microscopy. *Small* **2007**, *3*, 2011−2014.
(23) Iakhnenko, M.; Feyer, V.; Tsud, N.; Plekan, O.; Wang, F.; Ahmed, M.; Slobodyanyuk, O. V.; Acres, R. G.; Matolin, V.; Prince, K. C. Adsorption of Cytosine and AZA Derivatives of Cytidine on Au Single Crystal Surfaces. *J. Phys. Chem. C* **2013**, *117*, 18423−18433.
(24) Skomski, D.; Tempas, C. D.; Smith, K. A.; Tait, S.L. Redox-Active On-Surface Assembly of Metal-Organic Chains with Single-Site Pt(II). *J. Am. Chem. Soc.* **2014**, *136*, 9862−9865.
(25) Seljamae-Green, R. T.; Simpson, G. J.; Grillo, F.; Greenwood, J.; Francis, S. M.; Schaub, R.; Gano, J. E.; Fruchtl, H. A.; Lacovig, P.; Baddeley, C. J. Formation of Bioinorganic Complexes by the Corrosive Adsorption of (S)-Proline on Ni/Au(111). *Langmuir* **2015**, *31*, 262−271.
(26) Kong, H.; Yang, S.; Gao, H.; Timmer, A.; Hill, J. P.; Arado, O. D.; Monig, H.; Huang, X.; Tang, Q.; Ji, Q.; Liu, W.; Fuchs, H. Substrate-Mediated C-C and C-H Coupling after Dehalogenation. *J. Am. Chem. Soc.* **2017**, *139*, 3669−3675.
(27) Sigel, H.; Sigel, A. Metal Ions in Biological Systems: Nickel and Its Role in Biology. *Met. Ions Biol. Syst.* **1988**, *23*, 315−330.
(28) Sunderman, F. W. Recent Advances in Metal Carcinogenesis. *Ann. Clin. Lab. Sci.* **1984**, *14*, 93−122.
(29) Kawanishi, S.; Inoue, S.; Yamamoto, K. Site-Specific DNA Damage Induced by Nickel(II) Ion in the Presence of Hydrogen Peroxide. *Carcinogenesis* **1989**, *10*, 2231−2235.
(30) Besenbacher, F. Scanning Tunnelling Microscopy Studies of Metal Surfaces. *Rep. Prog. Phys.* **1996**, *59*, 1737−1802.
(31) Lægsgaard, E.; Osterlund, L.; Thostrup, P.; Rasmussen, P. B.; Stensgaard, I.; Besenbacher, F. A High-Pressure Scanning Tunneling Microscope. *Rev. Sci. Instrum.* **2001**, *72*, 3537−3542.
(32) Kresse, G.; Hafner, J. *Ab Initio* Molecular Dynamics for Open-Shell Transition Metals. *Phys. Rev. B: Condens. Matter Mater. Phys.* **1993**, *48*, 13115−13118.
(33) Kresse, G.; Furthmuller, J. Efficient Iterative Schemes for *Ab Initio* Total-Energy Calculations Using a Plane-Wave Basis Set. *Phys. Rev. B: Condens. Matter Mater. Phys.* **1996**, *54*, 11169−11186.
(34) Blöchl, P. E. Projector Augmented-Wave Method. *Phys. Rev. B: Condens. Matter Mater. Phys.* **1994**, *50*, 17953−17979.
(35) Kresse, G.; Joubert, D. From Ultrasoft Pseudopotentials to the Projector Augmented-Wave Method. *Phys. Rev. B: Condens. Matter Mater. Phys.* **1999**, *59*, 1758−1775.
(36) Perdew, J. P.; Burke, K.; Ernzerhof, M. Generalized Gradient Approximation Made Simple. *Phys. Rev. Lett.* **1996**, *77*, 3865−3868.
(37) Grimme, S.; Antony, J.; Ehrlich, S.; Krieg, H. A Consistent and Accurate *Ab Initio* Parametrization of Density Functional Dispersion Correction (DFT-D) for the 94 Elements H-Pu. *J. Chem. Phys.* **2010**, *132*, 154104.
(38) Ju, H.; Knesting, K.; Zhang, W.; Pan, X.; Wang, C.; Yang, Y.; Ginger, D. S.; Zhu, J. Interplay between Interfacial Structures and Device Performance in Organic Solar Cells: A Case Study with the Low Work Function Metal, Calcium. *ACS Appl. Mater. Interfaces* **2016**, *8*, 2125−2131.

DOI: 10.1021/acsnano.8b02821
ACS Nano XXXX, XXX, XXX−XXX